

Plasma-micropatterning of albumin nanoparticles: Substrates for enhanced cell-interactive display of ligands

María Pía Rossi

New Jersey Center for Biomaterials and Department of Chemical and Biochemical Engineering, Rutgers University, 599 Piscataway, New Jersey 08854

Jing Xu

Graduate Program in Cellular and Developmental Biology and Department of Biomedical Engineering, Rutgers University, 599 Piscataway, New Jersey 08854

Jean Schwarzbauer

Department of Molecular Biology, Princeton University, Princeton, New Jersey 08544

Prabhas V. Moghe^{a)}

Department of Chemical and Biochemical Engineering, Graduate Program in Cellular and Developmental Biology, and Department of Biomedical Engineering, Rutgers University, 599 Piscataway, New Jersey 08854

(Received 29 August 2010; accepted 11 October 2010; published 11 November 2010)

The authors demonstrate a novel, efficient, and widely applicable approach to direct the patterning of ligand-functionalized organic nanoparticles derived from albumin on nonconductive, biodegradable polymeric substrates. In contrast to traditional deposition methods for inorganic nanoparticles, the approach involves oxygen plasma treatment of spatially restricted regions on a nonbiopermissive polymer. Albumin nanoparticles conjugated with a truncated fragment of fibronectin containing the Arg-Gly-Asp domain were successfully patterned and used as templates to elicit adhesion and spreading of human mesenchymal stem cells and fibroblasts. Attachment and spreading of both cell types into the plasma-exposed polymer areas was considerably more pronounced than with the ligand alone. The authors hypothesize that the underlying mechanism is oxygen plasma treatment-induced selective enhancement of ligand exposure from the deposited functionalized nanoparticles, which facilitates ligand receptor clustering at the cell membrane. The results highlight a promising nanoscale approach to modulate ligand presentation and spatially direct cell attachment and phenotypic behaviors. © 2010 American Vacuum Society.
[DOI: 10.1116/1.3507236]

I. INTRODUCTION

The arrangement of living cells is crucial for the functionality of tissues during development and regeneration.^{1,2} The formation of functional tissues can result from optimal cell-cell and cell-extracellular matrix contacts, which frequently require the precise display of adhesion ligands. Extracellular matrix geometry and cell-matrix interactions, in particular, have been shown to play a crucial role in guiding cell fate and control processes such as apoptosis, proliferation, and differentiation.³⁻⁶ Therefore, considerable effort has been dedicated to manipulate the presentation of extracellular matrix ligands and proteins to spatially guide cell behavior.

One approach for spatially directing cell fate involves the creation of cell or protein patterns. Controlling the specific placement of cells is necessary in tissue engineering applications such as morphogenesis or networking,⁷ and patterned templates could be used for basic scientific research and provide mechanistic insights into cell attachment,⁶ migration,⁸ and cell-cell or cell-extracellular matrix communications.⁵ It could also lead to improvements in the development of de-

vices such as sensors,⁹ drug and protein screening tools,^{10,11} and microelectromechanical systems (MEMS).¹² Therefore, techniques, such as microcontact printing,¹³ micromolding in capillaries,¹⁴ dip-pen lithography,¹⁵ photolithography,¹⁶ and electron beam lithography,¹⁷ among others, have been used to pattern proteins,¹⁸ cells,¹⁹ and even bacteria.²⁰

Recently, interest in nanoscale presentation of ligands and proteins to manipulate cell function and fate has deepened; specifically, diverse types of nanoparticles are being explored for this application since these promote ligand presentation at the regimen over which receptor-ligand interactions occur. Previous research showed that presenting ligands and peptides in a clustered fashion results in the subsequent clustering of integrins, cell surface receptors, and promotes cell actions such as enhanced adhesion and motility.²¹ Therefore, nanoparticles are a natural means to present ligands, proteins, and peptides at the nanoscale, mimic ligand clustering, and promote integrin clustering to trigger or augment cell functions. For example, Cavalcanti-Adam *et al.*²² investigated the effect of ligand spacing on cell morphology and cytoskeletal organization by presenting Arg-Gly-Asp (RGD) peptides on gold nanoparticles at varying distances, and Mannix *et al.*²³ demonstrated the feasibility of using magnetic nanoparticles to actuate integrin clustering.

^{a)}Author to whom correspondence should be addressed; electronic mail: moghe@rutgers.edu

These studies have validated the use of ligand-functionalized nanoparticles to manipulate cell behavior, but there is a lack in the use of nanoparticles to spatially guide cell fate. To date, nanoparticle patterning has been explored mostly for electronic sensor and device applications, and nanoparticles made of silver,²⁴ gold,²⁵ and magnetic²⁶ materials have been successfully arranged into templates. These recent reports, however, are limited by the materials used, which are neither biodegradable nor amenable to bioactive remodeling. Thus, patterning of organic nanoparticles on biocompatible and bioresorbable materials remains a challenge and is the major topic for this study. Specifically, we sought to template biodegradable albumin nanoparticles on biocompatible but nonpermissive tyrosine-derived polycarbonates for spatial guidance of cells. We have previously established that substrates adsorbed with truly nanoscale albumin-derived carriers functionalized with cell adhesion ligands can affect cell adhesion and motility.²⁷ In this study, we demonstrate a technique to establish spatially controlled patterns of the albumin nanoparticles on nonpermissive polymer films by using microscale plasma-initiated patterning (μ -PIP), which uses oxygen gas plasma to etch polymer surfaces, to organize cell attachment and spreading. This platform of micropatterned nanoparticle substrates greatly sensitizes cell adhesion and morphogenesis to the presented ligands. Given the enhanced bioactivity of such biofunctionalized particles, such templated substrates could serve as effective model bio-interfaces for study of cell responses to organize ligands.

II. MATERIALS AND METHODS

A. Albumin nanoparticle synthesis

Albumin nanoparticles (ANPs) were synthesized by denaturing filtered (0.22 μ m filter, Fisher) human serum albumin (30% w/v, Sigma, St. Louis, MO) diluted to 1% (v/v) in phosphate buffer saline (PBS) through an increase in pH to \sim 10.6 by the addition of 0.1M NaOH and a subsequent slow increase in temperature to 80 °C. The temperature was maintained for 10 min and the solution was then rapidly cooled to room temperature in an ice bath. After maintaining the temperature at 25 °C for 10 min, the pH was decreased to \sim 5.9 using 0.1N HCl and the temperature was increased to 37 °C slowly, without stirring. Upon reaching the temperature, the solution was stirred in order to induce self-assembly of the denatured albumin into the nanoparticles. The solution was allowed to stir to allow for nanoparticles to aggregate and then incubated with 0.1% (w/v) iodoacetamide (Sigma, St. Louis, MO) at room temperature for 1 h to stop the reaction. The nanoparticle solution was dialyzed at 4 °C overnight [molecular weight cut-off (MWCO) 100 kDa] to remove any unreacted monomeric albumin and filtered again (0.22 μ m filter, Fisher) to remove large aggregates. Nanoparticle sizes ranged from 30 to 140 nm.

B. Fibronectin fragment production and purification

Albumin nanoparticles were functionalized with a truncated fragment of fibronectin that consists of the ninth and

tenth type III domains of the protein. Fibronectin, a dimeric glycoprotein, is involved in cellular processes such as adhesion, spreading, and migration, and can help regulate tissue processes such as wound healing.²⁸ Both the ninth and the tenth type III domains within the selected fibronectin fragment (FNf) associate with integrins, cell surface receptors, and trigger intracellular signaling related to cell spreading, growth, and migration.^{29–31} The FNf was produced as previously described by cloning fibronectin cDNA into a pGEX vector for expression as a glutathione-S-transferase fusion protein.²⁷ *Escherichia coli* cells were transformed with the protein construct and fusion proteins were separated from bacterial lysates by glutathione-sepharose affinity chromatography (GE Healthcare, Piscataway, NJ).

C. Albumin nanoparticle functionalization

The ANPs were functionalized with the FNf protein using bioconjugation and peptide chemistry techniques³² as described before.²⁷ Briefly, both FNf and ANP concentrations were measured using the BCA protein assay (Pierce, Rockford, IL). *N*-succinimidyl 3-(2-pyridyldithio)propionate (SPDP) (Sigma, St. Louis, MO), a heterobifunctional cross-linking agent, can react with the amine groups in the proteins to form an amide linkage at one end, while the 2-pyridyldithiol group at the other end can react with sulfhydryl residues to form a disulfide bond. The FNf and ANPs were separately reacted with the SPDP for 30 min at room temperature at a concentration of 500 μ M. The FNf was then reacted with dithiothreitol (DTT) for 30 min at room temperature at a concentration of 0.5 mg DTT/mg of FNf to form a free sulfhydryl group. The reacted protein and nanoparticles were then dialyzed (MWCO 6 kDa) overnight at 4 °C and the final concentration of each was again measured by BCA protein assay. ANP-SPDP and FNf-SPDP-DTT were then reacted together for 4–6 h at room temperature for functionalization and dialyzed (MWCO 100 kDa) overnight at 4 °C to remove any unreacted species. The final concentration of FNf and albumin in the FNf-ANPs was then determined using the enzyme-linked immunosorbent assay (ELISA) as previously described.^{27,33}

D. Cell culture

To test the biofunctionality of patterned nanoparticles and their effect on cell behavior, we used nanoparticle templates to pattern human mesenchymal stem cells and human fibroblasts. Human mesenchymal stem cells (MSCs) were purchased from Lonza (Lonza, Basel, Switzerland). Mesenchymal stem cells were harvested and cultured from normal human bone marrow. Cells were tested for purity by flow cytometry and for their ability to differentiate into osteogenic, chondrogenic, and adipogenic lineages. Cells were tested positive for CD105, CD166, CD29, and CD44, and negative for CD14, CD34, and CD45. Different lots of MSCs (MSCs derived from various donors) were used to exclude donor-dependency. Only passages earlier than eight were used in this study. Human mesenchymal stem cells (hMSCs) were cultured with a human mesenchymal stem cell media

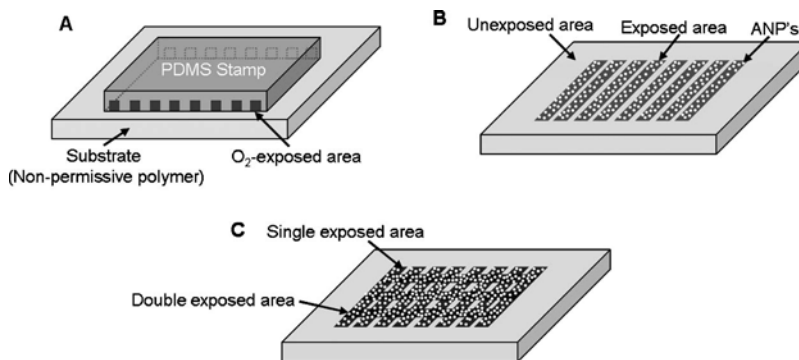


FIG. 1. Schematic illustrating the microscale plasma-initiated patterning process. (A) A PDMS stamp is placed on the biocompatible, bioresorbable polymer surface and treated in oxygen plasma at a pressure of 660 mTorr for 60–120 s and 50 W. Areas of the polymer exposed to the plasma undergo surface functionalization via the formation of end groups by interaction with the radicals, electrons, and ions in the oxygen plasma. (B) Biofunctional ANPs then preferentially adsorb to the exposed area of the material. (C) By exposing the polymer to the oxygen plasma for 60 s, rotating the stamp by 90°, and exposing the polymer to the oxygen plasma for 60 s again, areas of differentially exposed polymer enabled the differential deposition of nanoparticles for cell attachment.

kit (Lonza, Basel, Switzerland). Human fibroblasts were isolated from neonatal foreskin and cultured in McCoy's 5A medium (Invitrogen, Chicago, IL) supplemented with 10% fetal bovine serum, 1% Penicillin/Streptomycin (Biowhitaker, Walkersville, MD), and 1% L-glutamine (Invitrogen, Chicago, IL). Both cell types were supplemented with serum-free media during and at least 16 h prior to experimentation.

E. Establishment of micropatterned albumin nanoparticles

Poly(DTE-co-8% PEG_{1K} carbonate) was selected for patterning studies not only because of its biocompatibility but also because it inhibits both protein and cell attachment.³⁴ The polymer, in powder form, was diluted in a 98.5% v/v methylene chloride/1.5% v/v methanol solution at 1% w/v. The solutions were then spin-coated at 4000 rpm onto acid-cleaned glass coverslips to form thin films (~100 nm) of polymer on the glass. An elastomeric poly(dimethylsiloxane) (PDMS) stamp with parallel grooves 10–400 μm in width and 5–10 μm in height and open at both ends was then utilized to selectively expose areas of the polymer surface to oxygen plasma, as shown in Fig. 1(A). These sizes were specifically chosen to guide cell processes, which occur at the microscale, and confirm the functionality of the nanoparticles. The stamp was fabricated by pouring a Sylgard 184 silicone elastomer kit at a base weight to cross-linker weight ratio of 10:1 over lithographically created masters.³⁵ Therefore, while some of the substrates are protected by the PDMS stamp, the area under the grooves is exposed to the oxygen plasma. The polymer was treated at 50 W for 60–120 s to ensure sufficient functionalization. After plasma treatment, nanoparticle solutions were incubated on the polymer surface overnight at 4 °C to ensure binding and adsorption of the nanoparticles onto the substrate. A schematic of the resulting nanoparticle patterns is shown in Fig. 1(B).

More complex patterning was also induced by doing a double exposure of the surface to the plasma. In this case, a single pattern was formed by exposing the surface, with the

stamp, for 60 s at 50 W, as shown in Fig. 1(C). The stamp was then rotated by 90° and the surface was exposed to the plasma again for 60 s at 50 W. Nanoparticle solutions were again incubated on the polymer surface after treatment overnight at 4 °C. Consequently, crossed patterns, as shown in the schematic in Fig. 1(C), were obtained, where selected regions were either unexposed, exposed for 60 s (single exposed), or exposed for a total of 120 s (double exposed). Single and cross-patterning approaches allowed for the spatial organization of biofunctional nanoparticles into simple and more complex arrays, respectively.

F. Zeta-potential measurements of albumin nanoparticles

The surface charge of unfunctionalized and functionalized albumin nanoparticles was measured by dynamic light scattering using Zetasizer Nano ZS (Malvern, Westborough, MA). The nanoparticles were diluted in PBS at 1:10 and injected into the disposable folded capillary cells (Malvern, Westborough, MA) by a syringe. Three measurements were recorded at 20 s/sample at room temperature.

G. Cell patterning

To pattern human mesenchymal stem cells and fibroblasts, nanoparticle templates of sizes ranging from 10 \times 10 to 200 \times 200 μm^2 were prepared as described earlier and washed. Fibroblasts were trypsinized at 37 °C for 5 min, centrifuged at 1000 rpm for 5 min, and resuspended in trypsin neutralizing solution (Sigma, St. Louis, MO). Human mesenchymal stem cells were trypsinized at 37 °C for 5 min, neutralized by MSC growth medium, and centrifuged at 600 g for 5 min. Cells were then counted, diluted to 10–50 000 cells/cm², and cultured on the poly(DTE-co-8% PEG_{1K} carbonate) patterned with the biofunctional nanoparticles at a Fnf concentration of 2–20 $\mu\text{g}/\text{cm}^2$. As a control, patterning of the ligand alone was also done. After plasma treatment, as described above, the ligand was diluted in PBS to the same concentration and the substrates were incubated

with the solution at 4 °C overnight. Similarly, patterning with the whole-length fibronectin as a control was done for control at a concentration of 10 $\mu\text{g}/\text{cm}^2$. Substrates were then washed and cells were cultured at a cell seeding density of 10–50 000 cells/ cm^2 , as described above.

H. Visualization of cell adhesion on patterned ANPs

Cell seeding on the microscale patterns of the polymer-deposited nanoparticles was assessed by fluorescent labeling of fixed cells 6–24 h after seeding. For staining, cells were washed three times with Dulbecco's phosphate buffered saline (DPBS) with Ca^{2+} and Mg^{2+} , fixed with 3.7% formaldehyde for 15 min at room temperature, washed, permeabilized with 0.5% Triton X-100 in PBS for 15 min at room temperature, and washed again. Samples were then blocked with 3% calcein (obtained from fat-free, dry powdered milk, Sigma, St. Louis, MO) for 1 h and washed. For actin staining, cells were incubated with fluorescein phalloidin at a 1:200 dilution for 1 h at room temperature and washed. Finally, Vectashield with 4',6-diamidino-2-phenylindole (DAPI) was added to the samples for nuclear staining as well as to prevent bleaching.

I. Fluorescence imaging of ANP patterns

To visualize the organization of nanoparticles into patterns, fluorescence microscopy was employed. Nanoparticle solutions were first incubated on the micropatterned substrates overnight at 4 °C. Unbound nanoparticles were washed three times with PBS. ANPs were fixed in 3.7% formaldehyde for 15 min at room temperature, washed three times in DPBS with Ca^{2+} and Mg^{2+} , blocked with 3% calcein (obtained from fat-free, dry powdered milk, Sigma, St. Louis, MO), and washed again. Subsequently, they were incubated with antialbumin primary antibody produced in mouse (Sigma, St. Louis, MO) at a 1:1000 dilution overnight at 4 °C, washed three times, and incubated with fluorescein isothiocyanate (FITC)-conjugated Donkey antimouse IgG at a 1:200 dilution (Jackson Immunolabs, West Grove, PA) for 2 h at room temperature. The stained patterns were then washed again and stored at 4 °C. Staining was also performed with the antibodies in the absence of nanoparticles to test for nonspecific binding of the antibodies to the micropatterned substrates and to ensure that the patterns observed were a result of nanoparticle patterning and not antibody patterning (data not shown).

J. Atomic force microscopy of ANP patterns

The uniformity of nanoparticle organization was examined using atomic force microscopy (AFM). Briefly, ANPs were also incubated on the micropatterned substrates at 4 °C overnight. Unbound nanoparticles were washed three times and kept in PBS. A Bioscope III (Digital Instruments, Santa Barbara, CA) in fluid contact mode was then used to image the patterns in solution.

K. Scanning electron microscopy of ANP patterns

For scanning electron microscopy, the nanoparticle solutions were incubated on the substrates overnight at 4 °C and washed five times with distilled water to remove excess salts that could obstruct imaging. Samples were then allowed to dry at room temperature and sputter coated with gold-palladium. An Amray 1830 with a LaB₆ electron gun at 20 kV was employed for imaging.

L. Quantification of exposure of FNf, adhesive fibronectin fragment

To better investigate the surface presentation of the ligand on the patterned substrates, we measured their surface adsorption via ELISA. Specifically, an ELISA using anti-GST antibody was performed to quantify the differences in protein binding for GST-FNIII_{9–10} between untreated and plasma-treated poly(DTE-co-8% PEG_{1K} carbonate) coverslips. Untreated and plasma-treated poly(DTE-co-8% PEG_{1K} carbonate) cover slips were incubated overnight at 4 °C with either FNf-ANP or FNf at different dilutions to avoid oversaturating the substrate. FNf standards were made by diluting stock FNf to 20 $\mu\text{g}/\text{ml}$ with PBS and making 1:2 serial dilutions. Wells were washed five times with PBS to remove unbound ligand and incubated with blocking buffer (13% nonfat dry milk) for 1 h at 37 °C. After washing five times with PBS, substrates were incubated with rabbit anti-GST (70 ng/ml) (Sigma) for 1 h at 37 °C. Wells were washed and further reacted with an appropriate horseradish peroxidase-conjugated goat antirabbit antibody (1:40 000) (Sigma) for 1 h at 37 °C. Sigma-FAST OPD tablets (Sigma) were used according to manufacturer's protocol as a substrate for the detection of peroxidase activity. The color reaction was developed for 30 min and absorbance read at 450 nm on a multiwell plate reader. The levels of GST-FNIII_{9–10} conjugated to ANC were obtained by linear regression utilizing standard curve of FNf absorbances. The absorbance reading of the GST-FNIII_{9–10}-ANC was used to estimate the concentration of GST-FNIII_{9–10} necessary to elicit "equivalent levels" of GST-FNIII_{9–10} adsorbed using linear regression based on the standard curve of GST-FNIII_{9–10} absorbances.

M. Immunocytochemistry of integrin $\alpha_5 \beta_1$ receptors in patterned cells

MSCs can be spatially patterned onto 100 μm wide stripes where the FNf-ANPs were specifically adsorbed due to the discontinuous distribution of hydrophilic regions etched by plasma treatment. In the studies on integrin localization, cells were seeded in serum-free media and started to form obvious patterns after 16 h. Serum-free medium was chosen to avoid proteins and growth factors present in serum-containing media and to avoid any effect these may have to cell patterning. This ensured the isolation of the effect of the functionalized nanoparticles. The cells were fixed and permeabilized with 0.5% Triton X-100/PBS for 15 min at RT. After blocking, the samples were incubated overnight at 4 °C in mouse antihuman integrin α_5 (isotype: IgG_{2b}, sc-

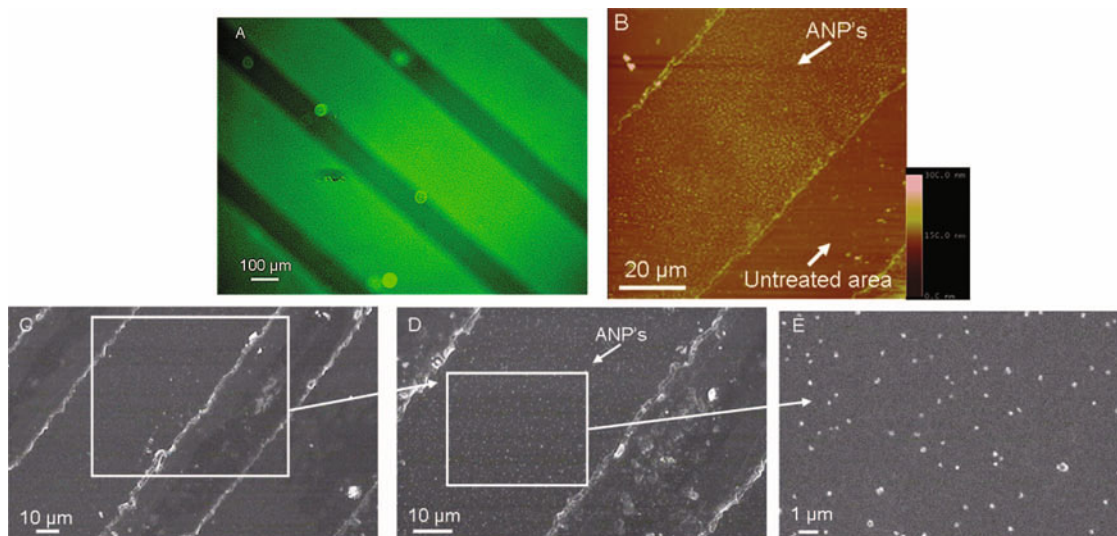


FIG. 2. (Color) Biointerfacial characterization of spatially restricted patterning of bioactive albumin nanoparticles. (A) Fluorescence microscopy image of patterned nanoparticles on poly(DTE-co-8% PEG1K carbonate). Briefly, after plasma-initiated patterning of the substrate with 660 mTorr oxygen at 50 W for 120 s, the nanoparticles were adsorbed onto the surface at 4 °C overnight, then washed, fixed, and stained with mouse antihuman serum albumin as a primary antibody and FITC-conjugated Donkey antimouse secondary antibody for visualization under fluorescence. (B) Atomic force microscopy image of nanoparticle patterns on poly(DTE-co-8% PEG1K carbonate). While nanoparticle monolayers are observed on one of the stripes (the plasma-exposed area), minimal nanoparticle adsorption is observed on the other stripes (unexposed or plasma-protected areas). (C) Scanning electron microscopy image of the nanoparticles patterned on the polymer substrates after plasma treatment. (D) High magnification scanning electron microscopy image of (C). (E) Higher yet magnification of plasma-treated region shows organization of nanoparticles in (D).

59761, Santa Cruz, USA) and antihuman integrin β_1 (isotype: IgG₁, sc-13590, Santa Cruz, USA), both at 1:100 dilution. After three washes with PBS, Alexa Fluor[®] 488 conjugated-antimouse IgG_{2b} and Alexa Fluor[®] 594 conjugated-antimouse IgG₁ antibodies (Invitrogen, USA) were added to visualize the antigens. Images were taken by the Nikon fluorescent microscope and Leica SP2 confocal microscope.

III. RESULTS

A. Nanoparticle pattern characterization

Figure 2(A) shows the stained pattern of the nanoparticles under fluorescence microscopy. The stamp used had a 400 μm stripe of exposed area by 100 μm of unexposed area; staining of the nanoparticles is observed on the 400 μm stripes, indicating that nanoparticles preferentially adsorb to the plasma-treated areas and do not adsorb onto the untreated areas. Figure 2(B) demonstrates nanoparticle patterning with atomic force microscopy. It is clear from the AFM that while nanoparticles form a monolayer on plasma-exposed regions of the polymer, they minimally adsorb to the unexposed areas of the polymer. The patterns were further confirmed with scanning electron microscopy, shown in Figs. 2(C)–2(E). Figure 2(C) shows two plasma-exposed stripes to which the ANPs preferentially adsorbed, with the unexposed stripes showing no nanoparticle adsorption. A higher magnification image, showing the nanoparticles adsorbed on one of the plasma-exposed stripes, is shown in Fig. 2(D), with a higher magnification image of the nanoparticles in the stripe shown in Fig. 2(E).

B. Fibroblast adhesion to micropatterned nanoparticles

We first chose to investigate the feasibility of nanoscale, biologically active ANP templating by creating patterns with primary fibroblasts.

Figure 3(A) shows the cell adhesion responses obtained with the patterned biofunctionalized nanoparticles when using a 40 \times 40 μm^2 stamp. In contrast to the patchy patterns obtained with the ligand alone [Fig. 3(D)], distinct patterns covering the entire stamped area can be obtained by using the ligand-functionalized nanoparticles. A higher magnification image of the patterns obtained with the functionalized nanoparticles [shown in Fig. 3(B)] demonstrates that cells remained highly confined to the plasma-exposed areas. Furthermore, it also can be seen that cells spread along the plasma-exposed area, in some cases even exhibiting a dendritic morphology. When patterning with ligand-functionalized nanoparticles, edge effects were not observed even when using a stamp with smaller features (10 \times 10 μm^2) that induced increased cell confinement, as can be seen in Fig. 3(C). In this case, the cells still spread throughout the striped area, instead of being confined to the edges of the plasma-treated areas, as is the case with the FNf patterns. Figure 3(D) shows the patterns that were obtained when using the ligand alone. It can be easily observed that the patterns were patchy, only forming in small areas scattered throughout the sample. Most cells spread on the substrate in a random, disorganized way. A higher magnification fluorescence microscopy image of the ligand-alone patterned areas [Fig. 3(E)] shows that cells are thin and elongated, not spread inside the plasma-treated area of 40 μm . In fact, the

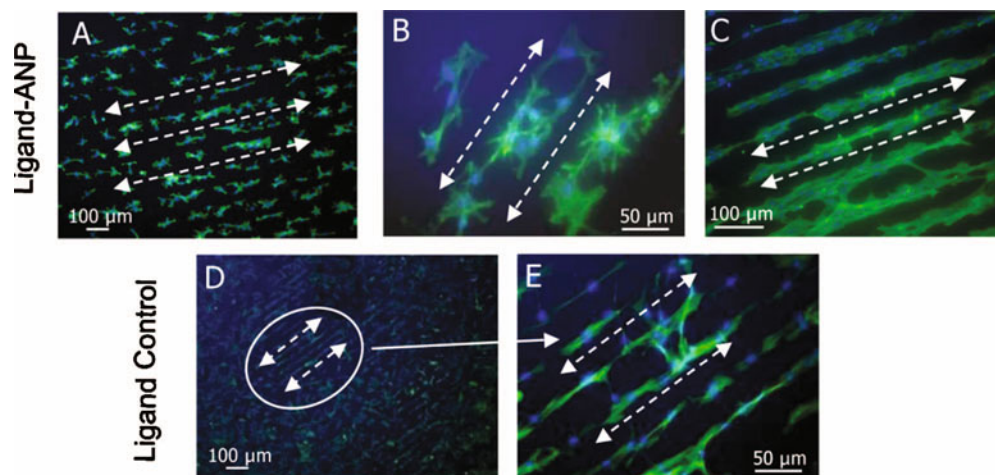


FIG. 3. (Color) Effect of spatially patterned bioactive, albumin nanoparticles on fibroblast adhesion and organization. (A) Fluorescence microscopy image showing how, in the presence of ligand-functionalized albumin nanoparticles, spatial arrangement of fibroblasts occurs across the $40 \times 40 \mu\text{m}^2$ stamped area, in comparison to the ligand alone, which formed patches of patterns. (B) Higher magnification fluorescent images show that cells spread across the pattern, adapting to the topography of the stripe. (C) Edge effects are not observed even by patterning using the $10 \times 10 \mu\text{m}^2$ stamp with the nanoparticles, despite the confined area. (D) Fluorescence microscopy image of fibroblasts patterned with ligand alone using a $40 \times 40 \mu\text{m}^2$ stamp. Patterning was sporadic and found only in small areas (green—actin; blue—DAPI). (E) Higher magnification fluorescence microscopy image of the fibroblast patterns with ligand alone suggests that cells elongate along the edges of the pattern rather than stretching along the entire plasma-exposed areas. Cells appear to be confined to the edges of the stripe.

patterned fibroblasts appear to be confined to the edges of the plasma-exposed polymer stripes, and the few patterns that were observed with the ligand alone may have resulted from the combination of the presence of protein and these plasma-exposed polymer edges rather than from patterned ligand. The optimal surface density of ANPs for both MSC and fibroblast cell attachment ranged from 3.5 to $4 \mu\text{g}/\text{cm}^2$.

The formation of more complex biological templates with functionalized ANPs was explored by cross-patterning. Serial exposure of stamped regions was achieved after rotating the stamp onto the polymer, as described earlier and shown in Fig. 1(C). In this more complex crossed-patterning, areas with different amounts of plasma treatment were created, where selected zones were either shielded from the plasma (i.e., unexposed), exposed for 60 s, or exposed for 120 s. As a result, when cell adhesion was examined, cells became arranged into square- and rectangularlike patterns, as shown

in Fig. 4(A), rather than the striped patterns shown in Figs. 3(C)–3(E). Higher magnification imaging [shown in Fig. 4(B)] indicates that the patterned areas are comprised of either single cells or a few cells that attached to and spread along while staying completely confined by the etched polymer areas. Double patterning with the ligand alone (control) was unsuccessful at eliciting more complex cell adhesion patterns, again validating the importance of patterning with biofunctionalized nanoparticles. As can be seen in Fig. 4(C), no cell confinement and no distinct patterns can be observed when the double-patterned substrates were incubated with the ligand solution.

C. Human mesenchymal stem adhesion to patterned nanoparticles

The effects of nanoparticle micropatterns were probed next using a different cell type, hMSCs. When culturing the

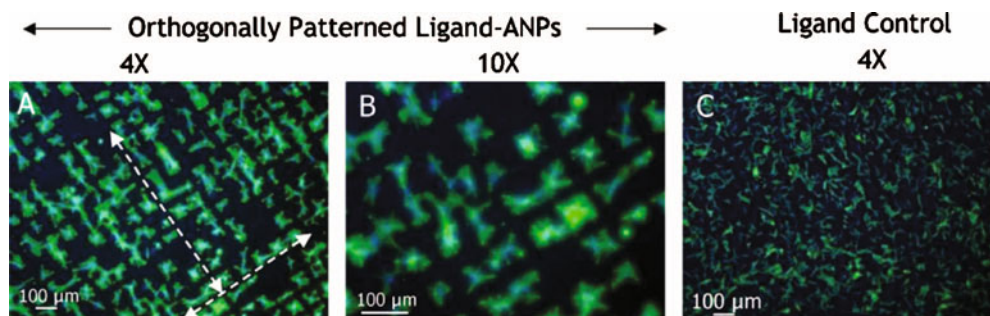


FIG. 4. (Color) More complex cell patterns can be obtained through differential deposition of albumin nanoparticles on polymer substrates. (A) Fluorescence microscopy image of fibroblasts double-patterned with ligand-functionalized nanoparticles. Double patterns were induced by exposing poly(DTE-co-8% PEG1K carbonate) spin-coated on glass cover slips for 60 s, then rotating the stamp by 90° , and exposing the polymer for another 60 s. (B) A higher resolution fluorescent image shows the cells adapting their morphology to the areas that were most exposed by plasma and appeared almost dendritic. (C) When using the ligand alone, no double patterning was observed.

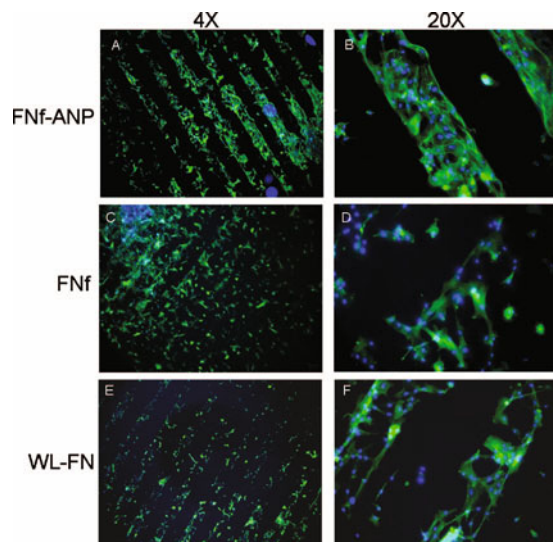


FIG. 5. (Color) Human mesenchymal stem cells adhere and organize effectively on spatially patterned albumin nanoparticles. Fluorescent images (green—actin; blue—DAPI) show MSCs patterned with FNf-functionalized albumin nanoparticles [(A) 4 \times ; (B) 20 \times], compared to those patterned on FNf fragment (control) [(C) 4 \times ; (D) 20 \times], and on positive control, whole-length fibronectin [(E) 4 \times ; (F) 20 \times]. Patterning with ligand alone, yields more contiguous organization than whole-length fibronectin control, and cells clearly spread within the plasma-exposed stripes [(C) and (D)].

hMSCs on the FNf-ANPs, well-defined patterns were observed [Figs. 5(A) and 5(B)], with the cells confined to the plasma-exposed areas exhibiting high levels of cell spreading. Figures 5(C) and 5(D) show hMSC patterning with the ligand, fibronectin fragment Fnf, alone at 4 \times and 20 \times magnification. Like the fibroblasts, hMSCs did not form distinct patterned areas on ligands deposited in the absence of nanoparticles and did not spread evenly within the plasma-exposed areas. Next, we compared effects of patterned bio-functionalized ANPs to those on patterned whole-length protein, fibronectin. Increased degree of cell spreading was observed when full length fibronectin was adsorbed onto plasma-treated polymer surface [Figs. 5(E) and 5(F)] in comparison to fibronectin fragment alone; however, the cell organization was not as contiguous as that on fibronectin fragment displayed from ANPs. Thus, presentation of a small recombinant fibronectin fragment (~ 50 kDa) from patterned nanoparticles could recapitulate cell adhesive behavior in relation to the fibronectin fragment and natural whole-length counterpart (~ 220 kDa).

D. Quantification of FNf exposure from micropatterned nanoparticles

Ligand adsorption of FNf and FNf-ANPs on untreated and plasma-treated poly(DTE-co-8% PEG_{1K} carbonate) was confirmed by ELISA (Fig. 6). The lower nanoparticle adsorption on the untreated polymer is caused by the presence of poly(ethylene glycol), or PEG, which inhibits protein, and subsequently nanoparticle, adsorption. Plasma treatment, however, increases the surface energy and negative charge

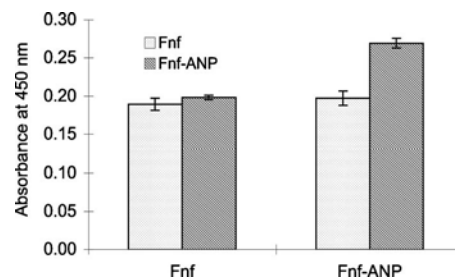


FIG. 6. Gas plasma treatment induces selective ligand exposure of functionalized albumin nanoparticles, but not for traditionally adsorbed ligand alone. ELISA studies confirm that the FNf-ANPs exhibit selective ligand patterning on plasma-treated poly(DTE-co-8% PEG_{1K} carbonate) substrates, a feature that was exploited to use FNf-ANPs as carriers to display otherwise nonselective ligand. The ligand FNf and FNf-ANPs at net equivalent amounts of ligand were deposited on untreated polymer spin-coated glass coverslips at approximately $1.53 \mu\text{m}^2/\text{cm}^2$. No statistical difference in ligand-alone adsorption was observed when comparing untreated poly(DTE-co-8% PEG_{1K} carbonate) and poly(DTE-co-8% PEG_{1K} carbonate) plasma-treated for 120 s, while plasma-treated polymer showed a significant increase in ligand exposure on FNf-ANPs.

on the surface of the polymer. The higher surface energy of poly(DTE-co-8% PEG_{1K} carbonate) is indicated by the completely wetting contact angle upon plasma treatment, in comparison to the contact angle of the untreated polymer of $69 \pm 2^\circ$.

The ELISA data showed that plasma treatment of the polymer induces greater levels of FNf exposure on FNf-ANPs. These data likely indicate that differences in adsorption or binding of the FNf-ANPs on untreated and plasma-treated surfaces induced differences in exposure of the ligand. As a result, plasma-exposed stripes expose higher ligand density than unexposed stripes, creating the cell patterns in a selective way. With the more uniform substrate coverage by the ligand alone, no cell patterning was induced.

E. Integrin mediated cell adhesion on micropatterned nanoparticles

We examined MSC cell adhesion to patterned FNf-ANPs in terms of the expression of the heterodimeric $\alpha 5$ and $\beta 1$ integrin receptors to fibronectin. Using immunolocalization with two distinct antibodies against integrin $\alpha 5$ and $\beta 1$ tagged secondarily with red and green fluorophores, respectively, we observed that cells adherent to micropatterned FNf-ANPs express colocalization of multiple integrin $\alpha 5$ and $\beta 1$. Several differences in the cell morphology were evident at higher magnification. Cells on FNf-ANPs showed more polygonal core shape and multiple smaller extensions, ending in knobbed lamellipodial ends, which were rich in colocalized integrins, whereas cells on FNf ligand (control) showed more extensive membrane elongation and branching, and the colocalized integrins, while visible throughout the cell body, were not pronounced at the ends of cell processes (Fig. 7).

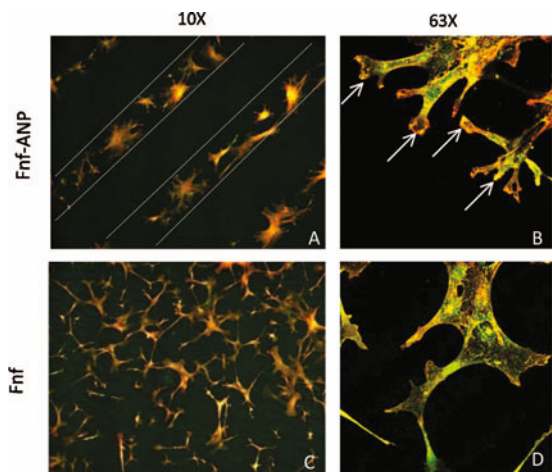


FIG. 7. (Color) Human MSCs adherent to micropatterned FnF-ANPs show distinct morphology and integrin α_5 and β_1 distribution visualized via immunolocalization and confocal microscopy. μ -PIP was used to spatially micropattern the functionalized nanoparticles [(A) and (B)] and the ligand alone [(C) and (D)]. Immunocytochemistry images (green—integrin β_1 ; red—integrin α_5) were taken at $10\times$ [(A) and (C)] and $63\times$ [(B) and (D)]. Note that cells patterned with FnF-ANPs (dashed lines) show more polygonal shape with numerous smaller peripheral extension where pronounced colocalization of integrin α_5 and integrin β_1 was observed the tips of pseudopodia (B). In contrast, cells on FnF controls showed restricted core spreading but extensive longer membrane processes and limited integrin colocalization at the pseudopodial tips [(C) and (D)].

IV. DISCUSSION

We sought to develop a platform to pattern organic nanoparticles onto bioresorbable polymers, with the goal of presenting biological cues for adhesion of cells. Our platform restricts the deposition of organic ANPs within plasma-treated regions on bioresorbable polymers that have limited levels of biopermissivity. The spatial treatment, termed as μ -PIP (Ref. 35), utilizes oxygen gas plasma to temporarily modify and functionalize the surface of materials.³⁶ Functionalization with oxygen gas plasma etches the polymer surface and increases the surface energy of the substrate.^{37,38} Specifically, the ionized gas oxidizes the polymer surface and induces the formation of $-\text{COO}^-$ and $-\text{CO}_3$ functional end groups that render hydrophobic polymers more hydrophilic.^{35,39,40} Poly(DTE-co-8% PEG_{1K} carbonate) was selected as the basally nonbiopermissive polymer due to the fact that it inhibits both protein and cell adsorption to the surface.^{34,41} Treatment of selected regions of the polymer with the oxygen plasma, however, increases the surface energy and hydrophilicity of the polymer, causing these regions to become permissive substrates for proteins and protein-based nanoparticles.

We examined the feasibility of establishing biological organization by using organic nanoparticles patterned on non-permissive, biocompatible substrates. The functionalized ANPs were previously shown to enhance the ability of human skin epithelial cells, called keratinocytes, to migrate²⁷ and induce accelerated assembly of fibronectin in the extracellular matrix by human fibroblasts,³³ two processes crucial to wound healing in the skin. In both studies, it was found

that cell response was enhanced by the presentation of the FnF from albumin-derived nanoparticles in comparison to presenting the FnF alone on the substrate. In this study, we proposed to use the FnF-functionalized albumin nanoparticles as the key model bionanoparticles for micropatterning studies. By fluorescence, atomic force, and scanning electron microscopy, we found that adsorption of ANPs is greater on plasma-exposed polymer in comparison to plasma-protected polymer. ELISA measurements showed that FnF adsorption was not statistically different in plasma-exposed and unexposed regions of the polymer, while ligand exposure on FnF-ANP was significantly enhanced in plasma-exposed regions than unexposed regions. Separately, we probed the interactions between the nanoparticle and the polymer substrate following plasma treatment of poly(DTE-co-8% PEG_{1K} carbonate). The zeta potential of the unfunctionalized nanoparticles and functionalized nanoparticles were $-(11.20 \pm 4.59)$ and $-(12.43 \pm 2.25)$, respectively, indicating that their surface charge is only slightly negative in PBS, and that ligand conjugation does not change the surface charge properties significantly. Using fluorolabeled nanoparticles, we found that the fluorescent intensity (RFI) of the albumin nanoparticles was 1613 ± 55 on untreated polymer, compared to 718 ± 17 on polymer pretreated with plasma for 120 s. The lower RFI value indicates a slightly lower amount of negatively charged nanoparticles adsorbed on the plasma-treated poly(DTE-co-8% PEG_{1K} carbonate). Therefore, we postulate that the modest repulsive effects of increased negative surface charge of plasma poly(DTE-co-8% PEG_{1K} carbonate) are outweighed by the increase in the surface energy and functionalization of the surface, promoting adsorption of the nanoparticles to the surface.

Patterning of the ANPs allowed for the spatial guidance of human mesenchymal stem cells and fibroblasts. Both cell types were not only confined to the plasma-exposed areas upon attachment, forming clear patterns, but they also spread within these regions; when patterning with the ligand alone, patterns of both cell types appeared patchy, and cells did not spread within the exposed areas. MSCs exhibited a distinct morphology on ligand-functionalized ANPs, characterized by polygonal core spreading and small peripheral extensions with knobbed ends, in contrast to the more restricted core spreading but longer extensions and branching on ligand controls. The nanoparticle substrates supported cell adhesion mediated by colocalized integrin α_5 and β_1 , which showed pronounced distribution in puncta at the ends of cell extensions. We believe that these effects resulted from a combination of enhanced ligand exposure induced by plasma treatment of ligand-specific integrin receptors, differences in nanotopography of the substrates, and integrin remodeling due to localized clustering. We have previously reported that the nanoscale ANP-based presentation can modulate, as a function of ANP nanoscale size, the cytoskeletal contractility and integrin translocation, which implicates synergistic effects of nanotopography and integrin distribution dynamics exerted by ligand presentation on albumin nanoparticles.^{33,42} Thus, spatially micropatterned ligand-functionalized nano-

particles could present effective tools to study and manipulate these processes in response to strategic ligands and varying nanoparticle features.

V. CONCLUSIONS

Patterning of cells is of interest for applications in tissue engineering, sensors and bio(MEMs) devices, among others. Confining cells to simple and complex patterns can help provide clues on cellular processes such as attachment, migration, and differentiation,³⁶ as well as cell-cell and cell-matrix interactions. However, while patterning with some proteins, such as fibronectin and laminin, has been successful, patterning with smaller ligands derived from the whole-length matrix proteins can be challenging and even unsuccessful, as shown here with a truncated fragment of fibronectin and RGD peptide.

By conjugating ligands on biocompatible, albumin-derived nanoparticles, it is possible to promote cell patterning using microscale plasma-initiated patterning. μ -PIP is a simple technique that can be used on nonconductive substrates for patterning of biodegradable, protein-based materials. Unlike microcontact printing, which can be patchy and is limited to materials of very specific surface chemistry, μ -PIP is very efficient for patterning a wider variety of materials. While we specifically chose microscale features because these range along the same size as cell processes, patterning depends on the features of the PDMS stamps, which can be tailored for nanoscale features. Aside from improving the presentation of ligands that do not preferentially adsorb to different substrates, patterning with nanoparticles could be helpful for presentation of ligands and proteins that undergo conformational changes due to interactions with the substrate, allowing them to retain activity.

ACKNOWLEDGMENTS

The authors would like to thank Jason Trager for the technical assistance, Bryan Langowski and Kathryn Uhrich for foundational work that inspired this study, Gary Monteiro for helping with AFM imaging, and Ram Sharma, Matthew Treiser, Rebecca Moore, and Vanesa Figueroa for helpful discussion. The authors gratefully acknowledge Joachim Kohn and the New Jersey Center for Biomaterials for the use of polycarbonate polymers. This work was funded by the NSF NIRT (Grant No. 0609000), NIH (Grant No. EB001046) (NIH NIBIB P41 Program on Polymeric Biomaterials: RES-BIO), and Rutgers Academic Excellence Fund. The project described was supported by Grant No. T32EB005583 from the National Institute of Biomedical Imaging and Bioengineering.

¹S. Bao and R. Cagan, *Dev. Cell* **8**, 925 (2005).

²T. Hayashi and R. W. Carthew, *Nature (London)* **431**, 647 (2004).

³M. A. Schwartz and M. H. Ginsberg, *Nat. Cell Biol.* **4**, E65 (2002).

⁴E. A. Cavalcanti-Adam, P. Tomakidi, M. Bezler, and J. P. Spatz, *Prog.*

Orthod. **6**, 232 (2005).

⁵J. M. Goffin, P. Pittet, G. Csucs, J. W. Lussi, J. J. Meister, and B. Hinz, *J. Cell Biol.* **172**, 259 (2006).

⁶D. Lehnert, B. Wehrle-Haller, C. David, U. Weiland, C. Ballestrem, B. A. Imhof, and M. Bastmeyer, *J. Cell. Sci.* **117**, 41 (2004).

⁷C. S. Chen, M. Mrksich, S. Huang, G. M. Whitesides, and D. E. Ingber, *Biotechnol. Prog.* **14**, 356 (1998).

⁸S. Li, S. Bhatia, Y. L. Hu, Y. T. Shiu, Y. S. Li, S. Usami, and S. Chein, *Biorheology* **38**, 101 (2001).

⁹C. Ziegler, *Fresenius' J. Anal. Chem.* **366**, 552 (2000).

¹⁰G. MacBeath and S. L. Schreiber, *Science* **289**, 1760 (2000).

¹¹C. J. Ziegler, A. P. Silverman, and S. J. Lippard, *J. Biol. Inorg. Chem.* **5**, 774 (2000).

¹²S. Lan, M. Veiseh, and M. Zhang, *Biosens. Bioelectron.* **20**, 1697 (2005).

¹³K. E. Schmalerberg, H. M. Buettner, and K. E. Uhrich, *Biomaterials* **25**, 1851 (2004).

¹⁴D. T. Chiu, N. L. Jeon, S. Huang, R. S. Kane, C. J. Wargo, I. S. Choi, D. E. Ingber, and G. M. Whitesides, *Proc. Natl. Acad. Sci. U.S.A.* **97**, 2408 (2000).

¹⁵K. B. Lee, S. J. Park, C. A. Mirkin, J. C. Smith, and M. Mrksich, *Science* **295**, 1702 (2002).

¹⁶L. M. Lee, R. L. Heimark, R. Guzman, J. C. Baygents, and Y. Zohar, *Lab Chip* **6**, 1080 (2006).

¹⁷G.-J. Zhang, T. Tani, T. Zako, T. Hosaka, T. Miyake, Y. Kanari, T. Funatsu, and I. Ohdomari, *Small* **1**, 833 (2005).

¹⁸J. D. Hoff, L. J. Cheng, E. Meyhofer, L. J. Guo, and A. J. Hunt, *Nano Lett.* **4**, 853 (2004).

¹⁹M. Veiseh, B. T. Wickes, D. G. Castner, and M. Zhang, *Biomaterials* **25**, 3315 (2004).

²⁰L. Xu, L. Robert, Q. Ouyang, F. Taddei, Y. Chen, A. B. Lindner, and D. Baigl, *Nano Lett.* **7**, 2068 (2007).

²¹G. Maheshwari, G. Brown, D. A. Lauffenburger, A. Wells, and L. G. Griffith, *J. Cell. Sci.* **113**, 1677 (2000).

²²E. A. Cavalcanti-Adam, T. Volberg, A. Micoulet, H. Kessler, B. Geiger, and J. P. Spatz, *Biophys. J.* **92**, 2964 (2007).

²³R. J. Mannix, S. Kumar, F. Cassiola, M. Montoya-Zavala, E. Feinstein, M. Prentiss, and D. E. Ingber, *Nat. Nanotechnol.* **3**, 36 (2008).

²⁴A. F. Koenderink, J. V. Hernandez, F. Robicieux, L. D. Noordam, and A. Polman, *Nano Lett.* **7**, 745 (2007).

²⁵P. M. Mendes *et al.*, *Langmuir* **20**, 3766 (2004).

²⁶B. Basnar, J. Xu, D. Li, and I. Willner, *Langmuir* **23**, 2293 (2007).

²⁷R. I. Sharma, M. Pereira, J. E. Schwarzbauer, and P. V. Moghe, *Biomaterials* **27**, 3589 (2006).

²⁸T. E. Petersen, H. C. Thogersen, K. Skorstengaard, K. Vibe-Pedersen, P. Sahl, L. Sottrup-Jensen, and S. Magnusson, *Proc. Natl. Acad. Sci. U.S.A.* **80**, 137 (1983).

²⁹H. Altroff, L. Choulier, and H. J. Mardon, *J. Biol. Chem.* **278**, 491 (2003).

³⁰A. L. Main, T. S. Harvey, M. Baron, J. Boyd, and I. D. Campbell, *Cell* **71**, 671 (1992).

³¹J. E. Schwarzbauer and J. L. Sechler, *Curr. Opin. Cell Biol.* **11**, 622 (1999).

³²G. Hermanson, *Bioconjugate Techniques* (Academic, New York, 1996).

³³M. Pereira, R. I. Sharma, R. Penkala, T. A. Gentzel, J. E. Schwarzbauer, and P. V. Moghe, *Tissue Eng.* **13**, 567 (2007).

³⁴E. Tziampazis, J. Kohn, and P. V. Moghe, *Biomaterials* **21**, 511 (2000).

³⁵B. A. Langowski and K. E. Uhrich, *Langmuir* **21**, 10509 (2005).

³⁶R. McBeath, D. Pirone, C. M. Nelson, K. Bhadriraju, and C. S. Chen, *Dev. Cell* **6**, 483 (2004).

³⁷J. R. Hall, C. A. L. Westerdahl, A. T. Devine, and M. J. Bodnar, *J. Appl. Polym. Sci.* **13**, 2085 (1969).

³⁸C. M. Chan, T. M. Ko, and H. Hiraoka, *Surf. Sci. Rep.* **24**, 1 (1996).

³⁹A. Khademhosseini, K. Y. Suh, S. Jon, G. Eng, J. Yeh, G.-J. Chen, and R. Langer, *Anal. Chem.* **76**, 3675 (2004).

⁴⁰B. A. Langowski and K. E. Uhrich, *Langmuir* **21**, 6366 (2005).

⁴¹S. I. Ertel and J. Kohn, *J. Biomed. Mater. Res.* **28**, 919 (1994).

⁴²R. I. Sharma, D. I. Shreiber, and P. V. Moghe, *Tissue Eng.* **14**, 1237 (2008).